

# DynSeizureGAT: Multi-band Dynamic Graph Attention Network for Interpretable Seizure Detection and Analysis of Drug-Resistant Epilepsy Using SEEG

Yiping Wang, Jinjie Guo, Ziyu Jia, Gongpeng Cao, Yanfeng Yang, Guixia Kang, Jinguo Huang

**Abstract**—The dynamic propagation of epileptic discharges complicates Drug-Resistant Epilepsy (DRE) seizure detection using traditional machine learning methods and Stereotactic Electroencephalography (SEEG). Several challenges remain unresolved in prior studies: (1) incomprehensive representations of epileptic brain network features; (2) lacking of flexible and dynamic mechanisms to learn brain network evolving features; and (3) the absence of model mechanisms interpretation corresponds with seizure mechanisms. In response, we propose a novel multi-band dynamic graph attention network, DynSeizureGAT, to detect and analyze DRE seizures with precision and interpretability. Specifically, a seizure network sequence is first constructed by integrating a multi-band directed transfer function matrix and enhanced epileptic index node features. Second, a dynamic graph attention module is integrated to dynamically weigh the contribution of various spatial scales. Third, spatial-spectral-temporal attention mechanisms enhance the model's capacity to better characterize and interpret the ictal and interictal states. Extensive experiments are conducted on the large-scale public clinical SEEG dataset (OpenNeuro). The proposed model demonstrates high seizure detection performance, achieving an average of 94.6% accuracy, 93.4% sensitivity, and 96.4% specificity. In addition, the importance of frequency bands and dynamic abnormal connectivity patterns is successfully quantified and visualized, which

contributes most to the explainability. Experimental results indicate that DynSeizureGAT demonstrates strong dynamic propagation feature learning capability, corresponding with seizure propagation mechanisms, and is promising to assist DRE epileptogenic zone localization.

**Index Terms**— Drug-Resistant Epilepsy, dynamic graph attention network, stereotactic electroencephalography (SEEG), seizure detection, interpretable analysis.

## I. INTRODUCTION

Drug-Resistant Epilepsy (DRE) cannot be effectively controlled with pharmacological therapy [1], increasing the risk of premature mortality due to seizure-related accidents, status epilepticus, and sudden unexpected death [2, 3]. Clinical treatment typically involves surgical resection or ablation to remove the epileptogenic brain tissue. The diagnostic process generally begins with non-invasive methods such as electroencephalography (EEG), multimodal neuroimaging, and neuropsychological evaluation [4]. However, when these techniques fail to provide consistent and accurate results, the advanced invasive technique stereotactic electroencephalography (SEEG) becomes necessary. SEEG is widely recognized as the "gold standard" for identifying the epileptogenic zone [5-8] and illustrated in Fig. 1, involves the placement of multiple deep electrodes into suspected brain regions to enable precise intracranial EEG monitoring and direct electrical stimulation. Therefore, monitoring and analyzing the differences between interictal and ictal signals are the first essential contents of SEEG diagnosis, which improves outcomes in epilepsy surgery. To address this clinical need, this work aims to develop more precise and interpretable methods for seizure detection and analysis using SEEG data to enhance DRE outcomes.

SEEG offers a significantly higher sampling rate compared to other EEG modalities, enabling more detailed pathological insights into the origins of epileptic seizures across temporal, spectral, and spatial dimensions. Epileptic biomarkers in temporal domain provide more discriminative information, such as spikes and pathological high-frequency oscillations (HFOs) [9]. Moreover, SEEG captures a broad frequency range from low-frequency rhythms to high-frequency oscillations, such as Ripple (R) in 80Hz to 250Hz and Fast Ripple (FR) in 250hz to 500hz, which are crucial for distinguishing normal brain activity and pathological signals. This wide frequency resolution provides a more comprehensive understanding for

This work was supported in part by the Beijing Natural Science Foundation under Grant L242097, and in part by the National Natural Science Foundation of China under Grant 62203063, and in part by the Tianjin Municipal Education Commission Scientific Research Project under Grant 2023KJ067, and in part by the Natural Science Foundation of China under Grant 82030037. This work was supported by the High-performance Computing Platform of Tianjin Medical University. We thank the NIH, JHH, UMMC, and UMF investigators for providing access to the data used in this study. (*Yiping Wang and Jinjie Guo contributed equally to this work.*) (*Corresponding authors: Yiping Wang; Jinguo Huang.*)

Yiping Wang is with the School of Biomedical Engineering and Technology, Tianjin Medical University, Tianjin, 300070, China (e-mail: ypwang@tmu.edu.cn).

Jinjie Guo, Gongpeng Cao and Guixia Kang are with the School of Information and Communication Engineering, Beiling University of Posts and Telecommunications, Beijing, 100876, China (e-mail: {Jinjieguo, gpcao, gkxkang}@bupt.edu.cn).

Ziyu Jia is with Beijing Key Laboratory of Brainnetome and Brain-Computer Interface, Institute of Automation, Chinese Academy of Sciences, Beijing, 100190, China (e-mail: jia.ziyu@outlook.com).

Yanfeng Yang is with the Xuanwu hospital of Capital Medical University, Beijing, 100053, China (e-mail: Yanfeng\_Yang@xwhosp.org).

Jinguo Huang is with the School of Intelligent Engineering and Automation, Beijing University of Posts and Telecommunications, Beijing, 100876, China (e-mail: hqj@bupt.edu.cn).

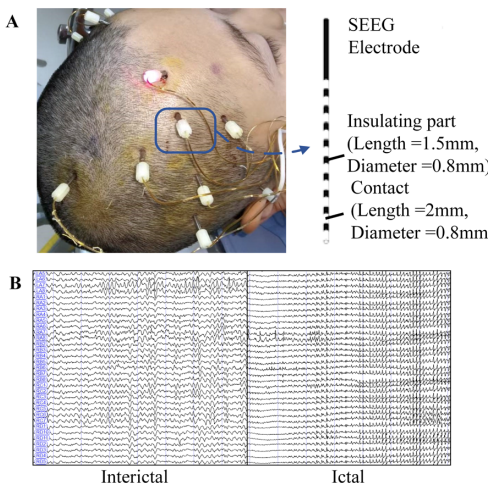


**Fig. 1.** (A) SEEG electrodes placed in the suspected epileptogenic area, the right side shows several contacts of an electrode. (B) Interictal and ictal SEEG signals.

dynamic changes of epilepsy activity. In the spatial domain, epileptic discharges rapidly propagates from epileptogenic regions to other brain regions, exhibiting a complex, instantaneous spatiotemporal dynamic process [10, 11]. Thus, the optimization of SEEG decoding methods is critical, in order to extract and interpret the dynamic, high-dimensional epileptic features.

Existing research shows that the international standard of detecting seizures is the visual identification of pathological discharges in the multi-channel SEEG by medical experts [7]. However, the visual inspection of continuous SEEG recordings is a time-consuming, error-prone process and misdiagnosis can be harmful, potentially leading to injury or even death [10, 12-14]. Typically, the research on this task using machine learning is conducted in three steps: (1) modeling the SEEG brain network, computed from an functional connectivity (FC) matrix representing pairwise dependencies between SEEG channels are often used, including local directional coherence analysis [15], directional transfer function (DTF) [16, 17] and information theory [18], among others; (2) extracting features of the brain network topology via statistics or graph-theoretic measures, such as in-degree, out-degree, and degree centrality [19, 20]; and (3) classifying the extracted features using machine learning algorithms[16, 21, 22], such as clustering algorithm. However, there are remains several significant challenges, such as incomprehensive representations of epileptic brain network features, lacking of flexible and dynamic mechanisms to learn brain network evolving features, and absence of interpretable model linking to seizure mechanisms.

The first step is to construct the individual seizure brain network. Intracranial brain network is typically constructed using leads as graph nodes and the effective connection relationships between brain regions as graph edges [23]. Graph node features are commonly defined as a statistical summaries of the signal in time domain [24], frequency domain [25], or differential entropy [8, 12], which is lack of the distribution of epileptic signals. Graph edge features are usually defined using FC measures, such as in [16, 25-27]. The brain graph can also be automatically learned by deep models [28, 29]. While such approaches are flexible and can converge to an optimal graph

structure for a given learning task, the learned brain graph may not represent the disease-specific pathological frequency band connectivity, for example, the R and FR band where the interictal period biomarkers are located. Therefore, a brain network modeling method that can benefit from the full spectral domain and the spatial domain is needed. Based on this motivation, we construct seizure brain network sequences with comprehensive and discriminative information, by decomposition of multi pathological frequency band for edge representation, and using epileptogenicity index features to enhance nodes feature.

The main purpose of the second and third steps is to model network features and classify the signals. Graph neural networks (GNNs) can simultaneously perform these steps, have introduced new directions in deep learning and graph-based data analysis [19, 30]. Dou et al. [31] used a graph convolutional network (GCN) to aggregate the features of connected neighboring contacts in a seizure localization task. Klepl et al. [28] proposed an adaptive gated GCN to weigh the contribution of various spatial scales in Alzheimer's disease EEG detection. Although these methods offer innovative ways of modeling complex relationships in data structures, there are limitations. On one hand, the traditional static graph model assumes fixed spatial and temporal relationships within EEG, failing to reflect the dynamic spatiotemporal topologies attributes of seizure brain activity, and on the other hand, it fails to effectively generalize across different patients or adapt to seizure individual variability.

To overcome the above static limitations, sliding windows are usually used to construct graph sequences in dynamic network feature learning. Our team [30] proposed an adaptive graph building and analysis block to integrate seizure detection and localization. Wang et al. [32] proposed a spatiotemporal graph attention network (STGAT) to explore spatial topological information in seizure prediction tasks. Zheng et al. [29] proposed a novel GNN architecture for analyzing dynamic brain connections, by leveraging dynamic variational autoencoders and spatiotemporal attention. Thus, the integration of GNN architecture and sequence modeling can capture the temporal dependency of dynamic GNN evolution, enables to improve the sensitivity of seizure detection[15, 29, 33, 34]. However, these studies are unable to flexibly adapt to the dynamic changes across different seizure phases, such as dynamic spatiotemporal topological features of the transition from interictal to ictal. Brody et al. [35] proposed a dynamic graph attention variant (GATv2) to address the limitations of static attention by modifying the order of operations. Therefore, our inspiration comes from the idea that dynamic GNNs and dynamic graph attention can more accurately represent evolving brain network features, while also adaptively addressing individual patient variability to a certain extent. Based on this motivation, after the first step of comprehensive seizure brain network modeling, we integrate dynamic sequential feature learning and dynamic attention mechanisms, to effectively model the better capture the evolution of seizures from spatial-spectral-temporal (SPT) dynamics seizures in SEEG and improve seizure detection accuracy.

Lastly, while developing seizure detection models with high accuracy is essential, it is equally crucial for these models to provide interpretable seizure localization information that can inform treatment strategies [14, 29, 36-38]. Model interpretability for GNNs remains a key challenge in this relatively new field, although early studies demonstrate the potential to advance this area, thereby improving both trust and clinical applicability. Specially, interpretability is essential for ensuring that a detection is made based on clinically proven epilepsy pathogenesis and for addressing the lack of transparency [39]. SEEG is characterized by SPT dimensions, and since all are crucial for seizure detection, an explanation of an algorithmic prediction should encompass these dimensions. The spatial dimension reflects the location in the deep brain [40], the spectral dimension refers to the frequency bands with significant differentiation between signals, and the temporal dimension refers to the point in time during the recording [41]. Therefore, we explain and analyze the model mechanism from multiple dimensions based on the previous interpretable model components.

To overcome the limitations in prior research and develop more precise and interpretable seizure detection and analysis methods using SEEG, we propose a novel method called DynSeizureGAT. In DynSeizureGAT, we model the task of seizure detection as a binary graph classification problem. This approach introduces several key advancements. First, representing SEEG as dynamic seizure networks sequence using multi-band directed transfer function analysis and epileptogenicity index feature enhancement, we aim to capture the comprehensive and discriminative information between different period. Second, the introduction of an advanced variant of graph attention networks, GATv2, allows for dynamic weighting of node connections' importance. Third, we incorporate an SPT attention mechanism that identifies and focuses on critical features across different brain regions, frequency bands, and time intervals, enhancing both interpretability and accuracy. We select fourteen DRE patients in a newer public OpenNeuro SEEG dataset [7, 42, 43], and have evaluated the high sensitivity and specificity of DynSeizureGAT. Besides its technological innovations, DynSeizureGAT can find abnormal connection patterns, by visualizing the dynamic connection changes of pathological brain networks, thereby assisting clinician to achieve more accurate and explainable seizure detection. It is also expected to assist in locating the epileptogenic brain and provide a scientific method for resection and ablation surgery.

## II. DATA

The dataset used in this study is obtained from OpenNeuro HUP iEEG epilepsy dataset (DS004100) [7, 42, 43], which includes data from 57 drug-resistant epilepsy patients who underwent intracranial EEG with subdural grid, strip electrodes or stereotactically placed depth electrodes at the Hospital of the University of Pennsylvania (HUP). Each patient also underwent subsequent received treatment with surgical resection or laser ablation. Electrophysiologic data for both interictal and ictal periods are available, along with electrode localizations in the

**TABLE I**  
DEMOGRAPHIC INFORMATION ABOUT THE 14 DRE PATIENTS.

Patient id	Sex	Age Onset /Age Surgery	Number of SEEG Contacts	Sample Rate	Outcome(Engel)	Number of Seizure	Target	Therapy
HUP116	F	42/59	50	500	1A	3	MTL	ABL
HUP117	M	12/39	49	500	1A	3	TEM	RES
HUP140	F	26/47	86	1024	1B	3	MTL	ABL
HUP141	M	14/30	113	500	1C	5	MTL	ABL
HUP142	M	15/30	108	500	1D	3	MTL	ABL
HUP144	M	5/31	111	500	1D	5	TEM	RES
HUP146	M	4/16	122	1024	1A	3	TEM	RES
HUP148	M	16/23	101	500	1A	5	TEM	ABL
HUP157	M	16/25	164	1024	1B	5	MTL	ABL
HUP160	F	15/45	102	1024	1A	3	TEM	RES
HUP163	F	32/42	156	1024	1D	3	MTL	ABL
HUP164	F	14/34	176	1024	1D	3	MTL	ABL
HUP177	F	5/42	172	500	1A	3	TEM	RES
HUP185	M	9/38	113	500	1A	5	MTL	ABL

Note: F, female; M, male; MTL, medial temporal lobe; TEM, temporal; ABL, ablation; RES, resection.

ICBM152 MNI space. SEEG signals are recorded and digitized at 500Hz or 1024Hz sampling rates using a referential montage and preprocessed to eliminate line noise. Electrode configurations and signal labels are determined by a multidisciplinary team of neurologists and neurosurgeons.

We select and analyze 14 patients who received SEEG investigations followed by epilepsy resection or ablation surgery. The patient inclusion criteria are as follows: (a) pathological is temporal lobe drug-resistant epilepsy (TL-DRE); (b) seizure-free post-surgery with an Engel1 outcome; (c) a minimum of six months of post-operative follow-up; (d) at least one recorded seizure exhibiting rhythmic activity. Detailed information about each patient is given in TABLE I.

## III. METHODS

### A. Problem Definition and DynSeizureGAT overview

SEEG seizure detection based on dynamic FC is regarded as a dynamic graph binary classification task. The goal is to construct a seizure brain network sequence  $\mathcal{G}$  and train a graph neural network model  $F$  to learn the representation of the dynamic graph for predicting seizure labels. Specifically, for a given patient, SEEG is represented as a set of dynamic graph sequence, expressed as  $\mathcal{G} = \{G_0, G_1, \dots, G_T\}$ . The graph sequence  $\mathcal{G}$  captures the evolution of the brain's functional connectivity. The model  $F$  learns the representation  $\{h_0, h_1, \dots, h_T\}$  to predict the corresponding label  $\hat{Y}$ :

$$\hat{Y} = F(\mathcal{G}) \quad (1)$$

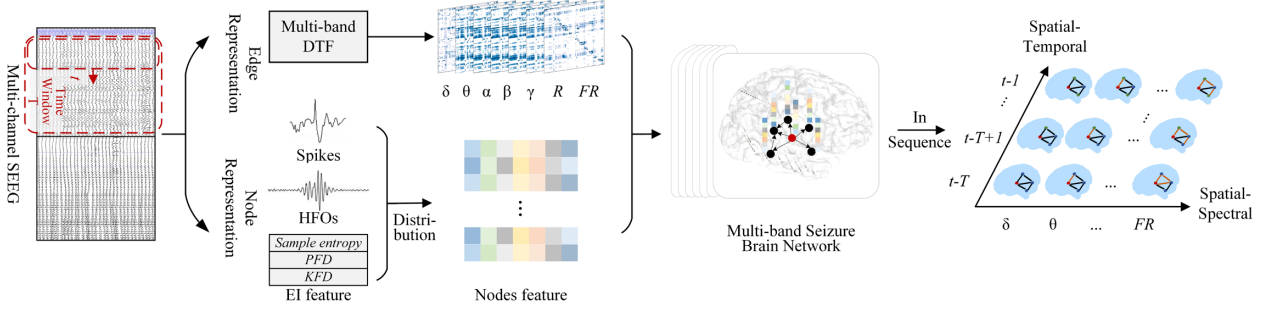
where  $\hat{Y}$  denotes the predicted label, categorizing the SEEG signal as either interictal or ictal.

Specifically, the model  $F$  refers to the proposed DynSeizureGAT, and the framework is illustrated in Fig. 2.

### B. Representing SEEGs as Multi-band Seizure Brain Networks Sequence

The method defines SEEG contacts as nodes, the connections between nodes as edges, and the direction as causality.

## A Seizure Brain Network Sequence



## B Dynamic Graph Representation and SPT Feature Learning

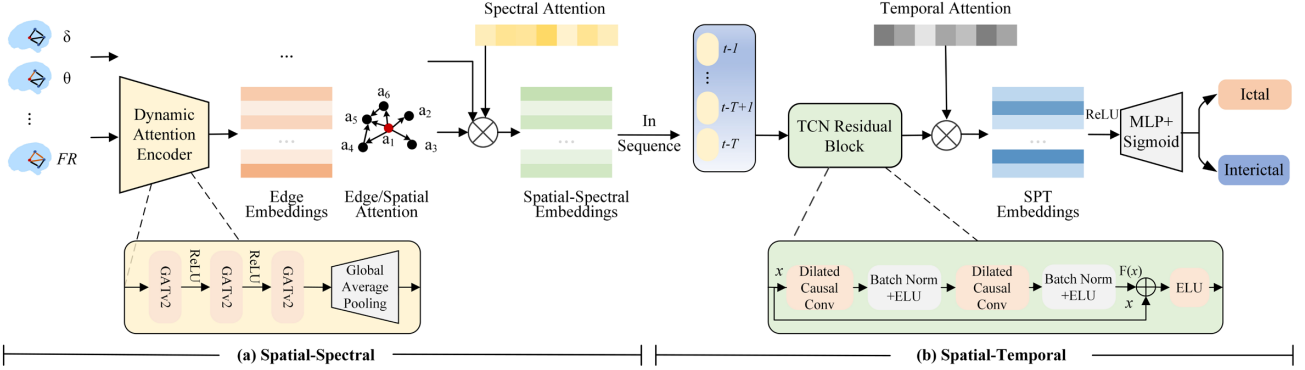


**Fig. 2.** The overall architecture of our proposed DynSeizureGAT. (A) To represent multi-channel SEEG as the seizure brain network sequence, we first leverage multi-band DTF analysis to represent the edges of SEEG functional brain networks. Then we extract node features based on the statistical distribution characteristics of spikes, HFOs, and EI feature. Finally, we arrange the multi-band seizure brain network into sequences by time order. (B) This module consisted of two parts. For spatial-spectral dynamic graph representation, we use the GATv2 mechanism to dynamically weight node connections based on their importance, enhancing the model's ability to focus on critical relationships. For SPT feature learning, temporal attention mechanism is combined with Temporal Convolutional Networks (TCN) to identify and focus on key features across time steps. Note: HFOs, high-frequency oscillations; PFD, petrosan fractal dimension; KFD, katz fractal dimension.

TABLE II

SEVEN DIFFERENT PATHOLOGY FREQUENCY BAND RANGES OF SEEG[11].

Bands	Frequency ranges (Hz)
δ	0.5~4
θ	4~8
α	8~14
β	14~30
γ	30~80
Ripple	80~250

Specifically, given a time window  $T$ , we represent the dynamic graph sequence as  $\mathcal{G} = \{G_0, G_1, \dots, G_T\}$ , and each SEEG clip  $t$  as a directed graph  $G = (V, E, W)$ , where  $V$  denotes the set of nodes (i.e., different SEEG contacts),  $E$  denotes the set of edges, and  $W$  is the functional connectivity matrix.

**1) Functional Connection Edge Representation based on Multi-band Directed Transfer Function:** The method focusses on seven different frequency band ranges of SEEG, as shown in TABLE II, calculates the weights of directed edges based on the DTF, and performs effective connectivity analysis between contacts.

The calculation of SEEG signals is performed within a time window of length  $T$  without overlap. First, a multivariate autoregressive (MVAR) model is constructed to calculate the estimated MVAR coefficients after obtaining dataset  $S$ . The specific calculation is built as follows:

$$\sum_{k=0}^p \Lambda(k)S(t-k) = E(t) \quad (2)$$

where  $\Lambda(0) = 1$ ,  $E(t)$  is a multivariate zero-mean vector. In Equation (2),  $p$  is the optimal model order, which is selected by the Akaike Information Criterion (AIC).

Second, the parameters are converted to the frequency domain to obtain  $\Lambda(f)$ , and the transfer coefficient matrix  $H(f)$  is derived at frequency  $f$  by inverting  $\Lambda(f)$ . An important property of  $H(f)$  is its asymmetry, which represents the directionality of the correlation. Based on the above definition, the causal effect of the records from the  $j$ -th region of interest on the  $i$ th region is expressed as:

$$\theta_{ij} = |H_{ij}(f)|^2 \quad (3)$$

Each estimated transfer function value is divided by the sum of the squares of all elements in the relevant row to obtain the normalized transfer function  $\psi_{ij}(f)$ . After normalization, the DTF values from region  $j$  to region  $i$  are obtained:

$$\phi_{ij}(f_1, f_2) = \sum_{f=f_1}^{f_2} \psi_{ij}(f) \quad (4)$$

where  $\phi_{ij}$  is in the range of  $[0, 1]$ ,  $\phi_{ij}(f_1, f_2)$  can exceed 1 in a broader frequency range.

Finally, the DTF matrix is sparsified, retaining the more important edges in the network and removing the edges with low weights. Specifically: 1) The diagonal element values are set to 0; 2) Edges with values lower than 25% of the total matrix value are set to 0, retaining only edges in the top 25% by weight. The parameter setting for the DTF matrix calculation, such as the model order is set to  $p = 10$  according to a heuristic

algorithm and comparative experience.

**2) Node Feature Representation based on Epileptogenicity Index:** We detect various epileptic electrical activities across different SEEG states using validated models and algorithms, such as spikes, high-frequency oscillations and significant numerical features. Then counts the occurrence rates of various epileptic activities and features at each contact to characterize the epileptic strength of the brain network nodes, thereby constructing a node feature matrix.

The specific process is as follows: First, we count the number of various epileptic electrical activities at each contact. For spikes count  $ns_i$  at contact  $i$ , the SEEG-Net model is used to load the optimal pre-training parameters for high-sensitivity detection of spikes, which has verified by the author [44]. The spike occurrence rate  $rs_i$  is expressed as:

$$rs_i = ns_i/T \quad (5)$$

where  $T$  is the time window length.

To more accurately detect HFOs number  $nh_i$  at contact  $i$ , three waveform types are included: ripples, fast ripples, and ripples and fast ripples co-occurring waves. For patients with a sampling frequency 500Hz, only ripples are detected. High-frequency oscillation events with more than six oscillations within a specified time window are identified according to the amplitude of the Hilbert envelope of the bandpass filtered signal, verified by the author [8]. The HFOs occurrence rate  $rh_i$  is expressed as:

$$rh_i = nh_i/T \quad (6)$$

Second, three significant numerical features of epileptogenic biomarkers in our previous study are used [8], sample entropy, petrosan fractal dimension (PFD) and katz fractal dimension (KFD). Specifically, the PFD and KFD calculate the fractal dimension in SEEG.

Finally, the node feature matrix is constructed to calculate the seven features within the time window  $T$ , representing the epileptic intensity coefficient of the node, or the weight degree of the vertex.

**3) Seizure Brain Network Sequence:** To capture the dynamic SPT epileptogenic features of the SEEG brain network, a seizure brain network sequence is constructed, with each representing the brain's state at a specific time step.

Snapshots of the dynamic graph are taken at equal intervals, resulting in a discrete sequence of network evolution, defined as  $\mathcal{G} = \{G_0, G_1, \dots, G_T\}$ , where each graph  $G_t = (V_t, E_t, X_t)$  represents the brain network at time step  $t$ . Here,  $G_t$  represents the brain network calculated at time step  $t$ ;  $V_t$  is the set of nodes (SEEG channels),  $E_t$  is the set of edges (connections calculated based on the DTF between channels), and  $X_t$  is the node feature matrix representing epileptic intensity.

### C. Dynamic Graph Representation Learning based on GATv2

The primary objective of graph representation learning is to build low-dimensional vector representations of nodes while preserving essential information, including SPT features. The seizure brain network sequence is input into an encoder, where the spatial-spectral correlations are extracted through dynamic GATv2 module.

**1) Static Graph Attention Problem:** GAT uses a self-attention mechanism in its hidden layers to assign individual weights to neighboring nodes during the aggregation process. The aggregation function is used in the message-passing step. Specifically, the attention coefficients  $\alpha$  are computed for each node-neighbor pair  $(i, j)$  and layer  $l$  by applying a feedforward neural network to the concatenated feature vectors of a node and its neighbors. The process is formalized in following:

$$h_i^{l+1} = \sigma(\sum_{j \in \mathcal{N}_i} \alpha_{ij} h_j^l) \quad (7)$$

$$e_{ij}^l = \text{LeakyReLU}(\vec{a}^T [W^l h_i || W^l h_j]) \quad (8)$$

$$\alpha_{ij}^l = \text{softmax}(e_{ij}^l) = \frac{\exp(e_{ij}^l)}{\sum_{k \in \mathcal{N}_i} \exp(e_{ik}^l)} \quad (9)$$

where  $\mathcal{N}_i$  represents the set of neighbors of node  $i$ ,  $e$  is the attention coefficients, and  $\alpha$  is the final attention coefficients obtained through a softmax function. This attention mechanism allows GAT to focus on the most relevant neighbors, enhancing node embeddings learning and improving performance on node classification tasks. Additionally, the attention weights contribute to model interpretability by highlighting important nodes in the network.

However, attention weights in GAT remain fixed based on initial characteristics, failing to adjust dynamically during training. This limitation hinders the model's ability to adapt attention weights based on changing relationships within the graph. This static attention mechanism results in nodes with similar initial attributes receiving identical attention, making it difficult for the model to account for dynamic relationships within the graph.

**2) GATv2 - Dynamic Graph Attention Mechanism:** To address this static graph attention problem, Brody et al.[35] proposed a dynamic graph attention extension that incorporated a second learnable attention matrix. This enhancement enables the dynamic update of attention weights throughout the training process, allowing the model to capture more complex and adaptive attention patterns.

To create a dynamic graph attention network, the internal operations in GAT are modified by introducing GATv2, a simple fix of GAT with a more expressive attention mechanism. GATv2 introduces a dynamic attention mechanism that facilitates more nuanced and adaptive learning. This modification involves reordering the operations in the GAT architecture such that the attention matrix is applied after a non-linear activation function. The attention score calculation is revised as follows:

$$e_{ij}^l = \vec{a}^T \text{LeakyReLU}([W^l h_i || W^l h_j]) \quad (10)$$

while this change was simple, it significantly improved the expressiveness and robustness of the model, particularly in handling noise. GATv2Conv resolves the limitation of collapsing learned layers into a single linear operation by introducing a more expressive attention mechanism. This modification significantly enhances the flexibility of the attention mechanism, allowing it to compute dynamic attention for any set of node representations. Moreover, by merging its linear layers, GATv2 can be computed faster than the original GAT model.

**3) Spectral Attention Mechanism:** After the above spatial

---

**Algorithm 1:** The Description of DynSeizureGAT.

---

**Input:** Raw multichannel SEEG data  
**Output:** The detection result of the model

- 1: Divide interictal and ictal SEEG into 1-second segments, labeling by seizure phase (interictal = 0, ictal = 1);
- 2: Compute the multi-band seizure network structure,  $G = (V, E, W)$ ;
- 3: Feed graph sequence  $\mathcal{G}$  and the ground truth label vector  $Y_t$  into the model as the training data  $D$ .
- 4: Initialize the predicted label vector  $\hat{Y}_t = 0$ .
- 5: **for** each sample  $(\mathcal{G}, Y_t)$  in  $D$  **do**
- 6:     **for**  $j$  in time-step **do**
- 7:         Hidden-state  $\leftarrow TCN(GATv2(\mathcal{G}), \hat{Y}_t)$
- 8:          $\hat{Y}_t \leftarrow$  Hidden-state
- 9:     **end for**
- 10:     $\hat{Y}_t \leftarrow softmax(W * \hat{Y}_t + B)$   $\triangleright W$  and  $B$  are parameters to be trained
- 11:    Calculate Loss according to (16).
- 12: **end for**

---

representation, the learned graph representation vector is weighted according to the seven frequency bands using the attention mechanism, which not only reduces the dimensionality of the data but also explains the importance of each frequency band for the classification of epilepsy periods. The attention calculation is expressed as:

$$v^t = U \tanh(W \mu_i + b) \quad (11)$$

$$\gamma^t = \frac{\exp(v^t)}{\sum_{j=0}^n v_j} \quad (12)$$

$$s_i = \sum_{t=1}^n \gamma_i \mu_i \quad (13)$$

where  $\mu_t$  represents the hidden layer input,  $v^t$  is the attention weight calculated from the network's output layer at time  $t$ , and  $\gamma^t$  represents the normalized attention weights, computed using learned weight parameters  $U$  and  $W$ , and bias  $b$ .

#### D. SPT Feature Learning based on TCN

In the proposed model, the Temporal Convolutional Network (TCN) module consists of one TCN layer and one self-attention layer. Compared to CNNs, TCN offers stronger temporal causality and a more flexible receptive field.

The TCN module consists of three main components: causal convolution, dilated convolution, and residual convolution. Causal convolution ensures strict adherence to the temporal order of the data. To address limited receptive field of causal convolutions, dilated convolutions are introduced, increasing the receptive field by incorporating a dilation factor  $d$ . The formula for dilated convolution is given as:

$$F(t) = \sum_{i=0}^{k-1} f(i) \cdot x_{(t-d \cdot i)} \quad (14)$$

Here,  $f(i)$  is the  $i$ -th convolution coefficient,  $k$  represents the size of the convolution kernel, and  $x_{(t-d \cdot i)}$  refers to the input data at time  $t$  dilated by  $i$ . Typically, the dilation factor is set to  $d = 2^i$ , where  $i$  is the layer index, with higher dilation factors expanding the receptive field.

To mitigate gradient vanishing problems, residual connections, dropout, and layer normalization are introduced in the TCN's residual module. These components create shortcut connections between layers, helping to maintain gradient flow and prevent vanishing. The residual connection is expressed as:

$$o = Activation(x + F(x)) \quad (15)$$

where  $x$  is the input,  $F(x)$  is the residual map to be learned, and  $o$  is the output. The SPT embeddings is then weighted with

**TABLE III**  
DETAILED RANGE OF PARAMETERS AND FINAL SPECIFICATION.

Parameters	Range	Final Value
GATv2 Layer	Num of Layers	[1,2,3,4]
	Embedding Size	[64,128,256,512]
TCN layer	Num of Layers	[1,2,3,4]
	Kernel Size	[1,2,3,4]
Learning Rate	Value	[1e-2,1e-3,1e-4]
	Weight Decay	[1e-3, 1e-4, 1e-5]
Batch Size	Value	[2,4,8,16]
	Num of epoch	[40,50,100]

**TABLE IV**  
CLASSIFICATION PERFORMANCE OF THE DYNSEIZUREGAT MODEL FROM SEIZURE DETECTION.

Patients	ACC(%)	SEN(%)	SPE(%)	PPV(%)	NPV(%)
HUP116	91.7	93.8	87.5	93.8	87.5
HUP117	100.0	100.0	100.0	100.0	100.0
HUP140	100.0	100.0	100.0	100.0	100.0
HUP141	95.7	93.3	100.0	100.0	88.9
HUP142	83.3	80.0	87.5	88.9	77.8
HUP144	100.0	100.0	100.0	100.0	100.0
HUP146	88.9	80.0	100.0	100.0	80.0
HUP148	91.7	87.5	100.0	100.0	80.0
HUP157	88.0	82.4	100.0	100.0	72.7
HUP160	100.0	100.0	100.0	100.0	100.0
HUP163	94.7	100.0	87.5	91.7	100.0
HUP164	94.4	90.0	100.0	100.0	88.9
HUP177	100.0	100.0	100.0	100.0	100.0
HUP185	96.0	100.0	87.5	94.4	100.0
<b>Average</b>	<b>94.6</b>	<b>93.4</b>	<b>96.4</b>	<b>97.8</b>	<b>91.1</b>

attention weights. Finally, classification is performed using an activation function.

#### E. Description of the DynSeizureGAT Algorithm

We define  $Y_t$  as the actual label vector and  $\hat{Y}_t$  as the predicted label vector. Equation 16 presents the model's loss function, where  $\theta$  represents the model parameters and  $\alpha$  denotes the regularization weight. The term  $\alpha \|\theta\|_2^2$  is included to prevent model parameter overfitting. The cross-entropy function calculates the inconsistency between the true label of the model and the predicted value.

$$Loss = Binary\_cross\_entropy(Y_t, \hat{Y}_t) + \alpha \|\theta\|_2^2 \quad (16)$$

Algorithm 1 provides a detailed description of the proposed seizure detection model.

## IV. EXPERIMENTS AND RESULTS

### A. Experimental designs

The OpenNeuro SEEG dataset consists of interictal (non-seizure) and ictal (seizure) signals, and is provided in BIDS format, which facilitates standardized data organization and processing. To improve the discriminative information, we remove the bad channels, and segment the data into 1-second for further analysis. We set the dynamic temporal step length to 7s, which is evaluated across ablation experiment in all patients, as shown in Fig. 3. The total data after segmentation is shown in Table S1.

TABLE V  
PERFORMANCE COMPARISON WITH OTHER EXISTING ALGORITHMS.

Authors	Graph Feature	Classifier	ACC(%)	SEN(%)	SPE(%)	PPV(%)	NPV(%)
Wang et al.,2020[26]	DTF	CNN	83.1	89.3	72.0	83.7	80.7
Shama et al.,2022[13]	Spatial Transformer	BiLSTM	85.1	87.0	80.5	89.1	80.0
Guo et al.,2021[45] & Grattarola et al.,2022[46]	IEEG-TCN	ECCbased-GNN	83.8	86.9	79.9	84.4	83.0
Klepl et al.,2023[28]	Adaptive feature	GCN-GRU	88.1	92.4	80.0	89.1	89.2
He et al.,2022[33]	Pearson correlation	GAT-BiLSTM	89.3	92.4	83.3	88.2	90.9
Wang et al.,2023[32]	Phase locking value	STGAT-GRU	90.9	93.3	86.3	92.3	89.6
<b>Proposed</b>	<b>Sparse DTF</b>	<b>STPGAT-TCN</b>	<b>94.6</b>	<b>93.4</b>	<b>96.4</b>	<b>97.8</b>	<b>91.1</b>

We evaluate each patient independently, each patient's data is randomly divided, 70% for model training, 20% for validation, and 10% reserved for evaluation. To evaluate the performance of DynSeizureGAT and baselines, the model parameters are determined based on multiple comparative experiments, and the parameter ranges and final specifications are shown in TABLE III. The Adam optimizer is selected to optimize model. The model implements with Pytorch and trains on Nvidia 3090 GPU.

To evaluate the performance, we use accuracy, sensitivity, and specificity. These metrics provide a comprehensive evaluation, capturing both its ability to correctly identify seizures (sensitivity) and to avoid false positives (specificity).

$$\text{Accuracy(ACC)} = \frac{TP+TN}{TP+FP+TN+FN} \quad (17)$$

$$\text{Sensitivity(SEN)} = \frac{TP}{TP+FN} \quad (18)$$

$$\text{Specificity(SPE)} = \frac{TN}{TN+FP} \quad (19)$$

$$\text{Positive Predictive Value(PPV)} = \frac{TP}{TP+FP} \quad (20)$$

$$\text{Negative Predictive Value(NPV)} = \frac{TN}{TN+FN} \quad (21)$$

Here, true positive (TP) refers to ictal signals correctly identified, true negative (TN) represents interictal signals correctly identified, the false positive (FP) represents incorrectly identified as ictal signals, and the false negative (FN) represents incorrectly identified as interictal signals. SEN and SPE represent the proportion of correctly identified ictal and interictal signals, respectively. PPV and NPV measure the accuracy of positive predictions and negative predictions.

### B. Classification performance of DynSeizureGAT

This section presents the performance of DynSeizureGAT in SEEG seizure detection. TABLE IV presents the average classification results for each patient (calculated from all seizures) and the overall results across the entire dataset. DynSeizureGAT achieves an average accuracy of 94.6%, sensitivity of 93.4%, and specificity of 96.4%. Additionally, with an average PPV of 97.8%, the model demonstrates a robust ability to predict true seizures when classifying a signal as ictal (seizure). This indicates that when the model detects a seizure, its predictions are highly accurate, effectively minimizing false positives. The model also performs well in predicting non-seizure states, achieving an average NPV of 91.1%, thereby ensuring that when it predicts a non-seizure state, the prediction is highly reliable. This performance gain is attributed to the seizure brain network sequence construction, the GATv2 block, and SPT attention, which play a vital role in simultaneously learning the spatial-spectral-temporal patterns of the dynamic epileptic brain.

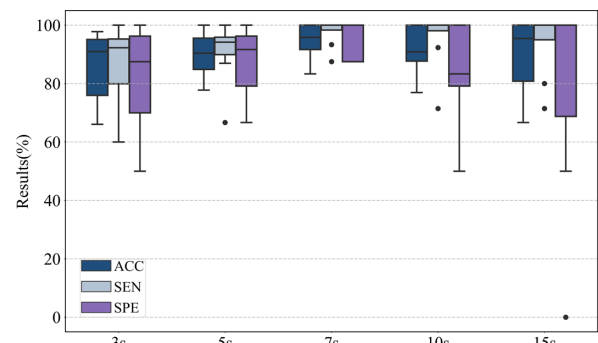


Fig. 3. Results of different dynamic sequence length with all patients. We keep DynSeizureGAT unchanged and use all patients for comparative analysis. The 7-second window provides the optimal balance predictions.

### C. Comparison with State-of-the-Art Algorithms

To demonstrate the advantages of the DynSeizureGAT model, we compare its average classification performance with other models using the selected 14 TL-DRE patients from the OpenNeuro SEEG dataset. All models are trained and tested under identical conditions to ensure a fair comparison. TABLE V presents a comparison of our method's average performance with CNN-based, RNN-based, GNN-based and GNN-RNN-based models, including CNN [26], BiLSTM [13], IEEG-TCN [45] with ECC-based GNN [46], GCN-GRU [28], GAT-BiLSTM [33], STGAT-GRU [32].

Our method achieves the best classification performance compared to other models and also shows a significant advantage in specificity. A noteworthy phenomenon is the relatively low classification performance of in the CNN-based and RNN-based models, with only about 83.1%-85.1% classification accuracy and 72.02%-80.5% specificity, compared to the better performance of GNN-based and GNN-RNN based models. The difference suggests that GNN-based models better fit the characteristics of spatial information. Furthermore, the results of GNN-RNN-based models show improvements across various indicators, indicating that spatial information changes over time are effectively modeled, consistent with the interpretation results with seizure mechanisms.

### D. Ablation study

To better understand the contributions of the DynSeizureGAT model's components, we conduct a series of ablation studies focusing on dynamic sequence length, brain network attributes, and model architecture.

**1) Impact of Dynamic Sequence Length:** To evaluate performance across different dynamic sequence lengths and

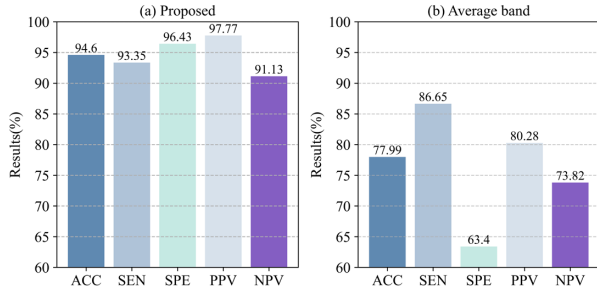


**Fig. 4.** The compared results using average frequency bands against multiband frequency bands. The figure shows that replacing the multi-frequency graph with a full-band graph led to a decrease in accuracy, sensitivity, and specificity.

**TABLE VI**  
PERFORMANCE COMPARISON WITH CONTRIBUTION OF VARIOUS NODE FEATURES.

Statistical distribution		ACC (%)	SEN (%)	SPE (%)	PPV (%)	NPV (%)
Spikes	HFOs	EI Features				
✓		83.8	87.4	76.3	88.8	73.8
	✓	86.7	91.9	80.4	89.2	85.0
✓	✓	88.5	89.7	81.3	90.8	87.1
✓	✓	92.1	92.7	89.6	96.3	88.3
✓	✓	89.8	91.9	88.4	94.1	84.3
✓	✓	94.6	93.4	96.4	97.8	91.1

determine the optimal evaluation window, we compute scores for all patients. Fig. 3 shows that a 7-second window provides the optimal balance between capturing features for accurate predictions and avoiding overfitting. From 3 to 7 seconds, accuracy and sensitivity steadily improve, with the highest performance observed at 7 seconds, achieving averages of 95.7% and 95.1%, respectively. However, accuracy declines beyond 7 seconds, suggesting that the model becomes overfitted, capturing noise. Specificity also declines sharply at 10 and 15 seconds, dropping to 82.0% and 78.3%, respectively, confirming that overfitting becomes a major issue at these extended intervals.

**2) Effectiveness of Seizure Brain Networks:** To further explore the impact of seizure brain network attributes on DynSeizureGAT, we conduct two ablation experiments focusing on frequency band decomposition and node feature representation.

We compare results using average frequency bands against multi-band frequency bands to assess the necessity of frequency band decomposition. Replacing the multi-frequency graph with a full-band graph led to a decrease in accuracy, sensitivity, and specificity, as shown in Fig. 4. This highlights the importance of capturing frequency-specific information in SEEG signals, which is crucial for accurately detecting seizures manifesting differently across frequency bands. The multi-frequency approach provides a richer representation, allowing the model to capture subtle frequency-specific patterns associated with seizure onset and propagation.

Furthermore, to investigate the contribution of various node features and identify the most informative feature set, we conduct feature ablation. The frequency decomposition and model classifier remained unchanged, as shown in TABLE VI. Using only HFOs improves performance contrasting with only

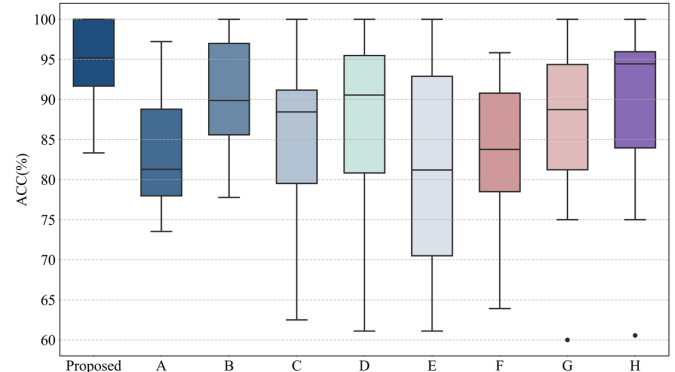


**Fig. 5.** Results of ablation experiments. The decrease ACC in A and B proves the superior spatial feature learning performance of the GATv2, and the decrease ACC in C and D proves the better temporal fitting performance of TCN.

spikes occurrence rate with an ACC of 86.7%, SEN of 91.9%, and SPE of 80.4%, indicating more balanced prediction reliability compared to using spike occurrence rate alone. The combination of spikes and HFOs demonstrates the best performance among two-feature combinations, indicating a strong ability to identify both ictal and interictal. Incorporating all three statistical distribution features achieve the highest performance. The inclusion of EI, in particular, consistently boosts specificity and PPV, underscoring its critical role in improving the reliability of ictal predictions.

**3) Effectiveness of Graph Representation Model:** We conduct ablation experiments to assess the contribution of each module in the proposed model. The following seven GNN-RNN-based ablated variants are tested:

- A: GATv2 replaced with GCN layers;
- B: GATv2 replaced with GAT layers;
- C: TCN Layer replaced with an MLP layer;
- D: TCN Layer replaced with a BiLSTM layer;
- E: variants A and C combined;
- F: variants A and D combined;
- G: variants B and C combined;
- H: variants B and D combined.

The ablation results in Fig. 5 reveal that each module contributes significantly to the architecture's performance. For variant A, performance dropped significantly, with accuracy falling to 86%. GCNs lack a focus on the most relevant nodes and edges, resulting in a loss of precision in capturing critical spatial relationships. For variant B, although GAT layers include attention mechanisms, they are less flexible than GATv2 in adapting to dynamic graph structures, which is essential for modeling SEEG data's variability over time. Furthermore, this module enables the production of explainable predictions. Next, we demonstrate that the TCN encoder significantly outperforms MLP layer and the BiLSTM encoder, as shown in variant C variant D. Performance decreases significantly when the temporal feature learning module is replaced with an MLP layer. While Bi-LSTM is designed for sequence modeling, they are prone to issues like vanishing gradients and may struggle with long-range dependency modeling compared to TCNs, which are also more computationally efficient. The TCN layer avoids the above problems, and has higher computing efficiency and more flexibility.

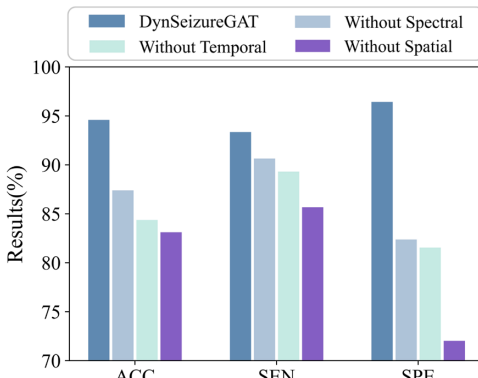


**Fig. 6.** Results of each attention component's impact.

Since all major modules contribute significantly to the model's final performance, it is unsurprising that the remaining ablated models, with more than one module modified, also perform significantly worse (Variants E-H in Fig. 5).

Overall, the ablation results clearly demonstrate that each module in the DynSeizureGAT architecture significantly enhances overall performance. Specifically, the GATv2 layers are essential to determine the importance of brain connections, highlighting critical connections between ictal and interictal. The module has captured dynamic abnormal connectivity patterns, such as the bidirectional extensive diffusion feature of the ictal network, and the unidirectional flows from the medial temporal lobe region to other structures in the interictal network. The spectral attention mechanism captures the important frequency bands where the significant patterns of ictal period, such as sharp activity and LVFA, as well as the important frequency bands where the significant patterns of interictal period, such as HFOs. While the TCN layers are crucial for modeling temporal dependencies in SEEG signals, its learned temporal dependencies are crucial for detecting the sequence of ictal events. Moreover, the superior performance of the full model over ablated variants underscores its potential as a valuable tool in clinical applications for DRE assisted diagnosis.

**4) Effectiveness of SPT attention mechanism:** As shown in Fig. 6, the ablation results demonstrate the distinct roles of the SPT attention mechanisms. Removing spatial attention by replacing GATv2 with GCN layers, results in a clear performance drop. Accuracy decreases from 94.60% to 83.11%, and specificity from 96.43% to 72.02%. This highlights the importance of spatial attention in modeling inter-regional interactions. Replacing the temporal and spectral attention modules with MLP layers also reduces performance. Without temporal attention, accuracy drops to 84.37%. Without frequency attention, accuracy drops to 87.40%, along with a decline in specificity. These results confirm that each attention component contributes uniquely. Spatial attention captures spatial dependencies, while temporal and spectral attention identify seizure-related patterns across time and frequency.

## V. DISCUSSION

### A. Dynamic Feature learning of DynSeizureGAT

In this work, DynSeizureGAT model is proposed for detecting and interpreting seizure brain states, such as ictal and interictal. The proposed model is evaluated on a public SEEG

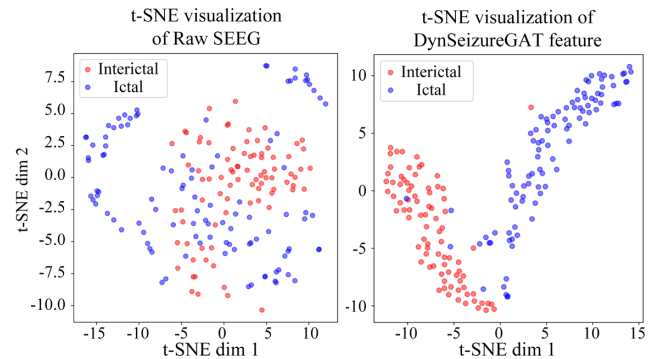


**Fig. 7.** Two-dimensional t-SNE visualization of feature distribution for both raw SEEG and dynamic features.

dataset, and achieved an average accuracy of 94.6%, sensitivity of 93.4%, and specificity of 96.4%, which is very outstanding classification performance compared with many existing methods. DynSeizureGAT offers two major contributions of dynamic feature learning from the perspective of novel model structure designation.

First, the model constructs SEEG seizure brain network sequences by decomposition of multi pathological frequency band for edge representation, and using epileptogenicity index features to enhance nodes feature. On the one hand, the decomposition can reflect the different frequency bands commonly analyzed in TL-DRE, and can focus on when making decisions. The pathological signal patterns corresponding to different frequency bands, making the brain network sequence representation more comprehensive and discriminative. On the other hand, the nodes feature enhancement based on epileptogenicity index integrate statistical distribution features of high-frequency oscillations, spike frequencies and significant numerical features to improve accuracy and interpretability.

Second, the model integrates GATv2 module, SPT attention and TCN to dynamically weigh the contribution of various spatial scales, frequency band and time steps. The GATv2 module is introduced to perform dynamic graph representation and learn the importance of brain connections, highlighting critical brain connections for differentiating ictal and interictal. This GATv2 reorders the operations in the GAT architecture such that the attention matrix is applied after a non-linear activation, which enables the dynamic update of attention weights throughout the training process, allowing the model to capture more complex and adaptive attention patterns, and can be computed faster than the original GAT model. This analysis provides high accuracy and interpretability by capturing connectivity between different regions and significant frequency band between different period.

To deeper understand the insights of the dynamic feature learning ability of DynSeizureGAT, we use the t-distributed stochastic neighbor embedding (t-SNE) algorithm [47] to visualize the distribution of both raw SEEG and dynamic features. Fig. 7 presents the two-dimensional t-SNE results of patient HUP177. As observed, the dynamic features of DynSeizureGAT show a clearer separation between categories, highlighting the model's strong class-discriminative performance.

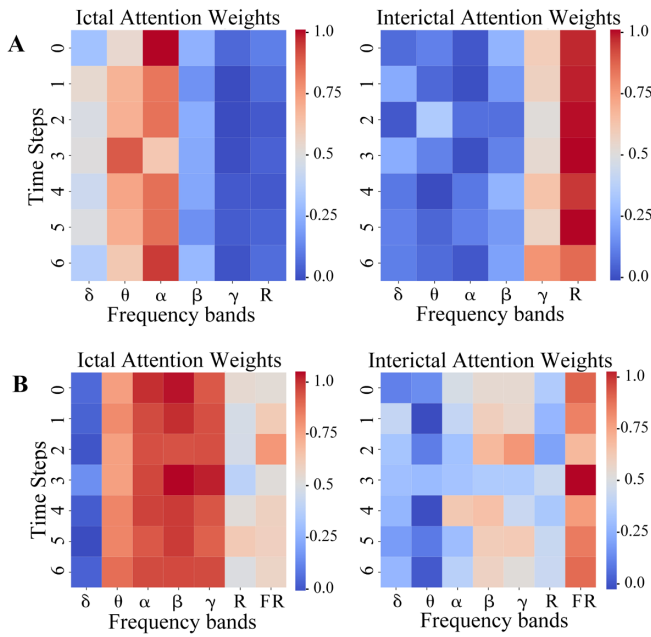


**Fig. 8.** Visualization of multi-band spectral attention weight values in ictal and interictal period, where A is patient HUP177 and B is patient HUP160.

### B. Interpretable DynSeizureGAT corresponds with Seizure Mechanisms

In this section, we interpret DynSeizureGAT based on the model learning process analysis and corresponding to DRE seizure mechanisms. Specifically, we identify important frequency bands and dynamic abnormal connectivity patterns by quantifying and visualizing their importance.

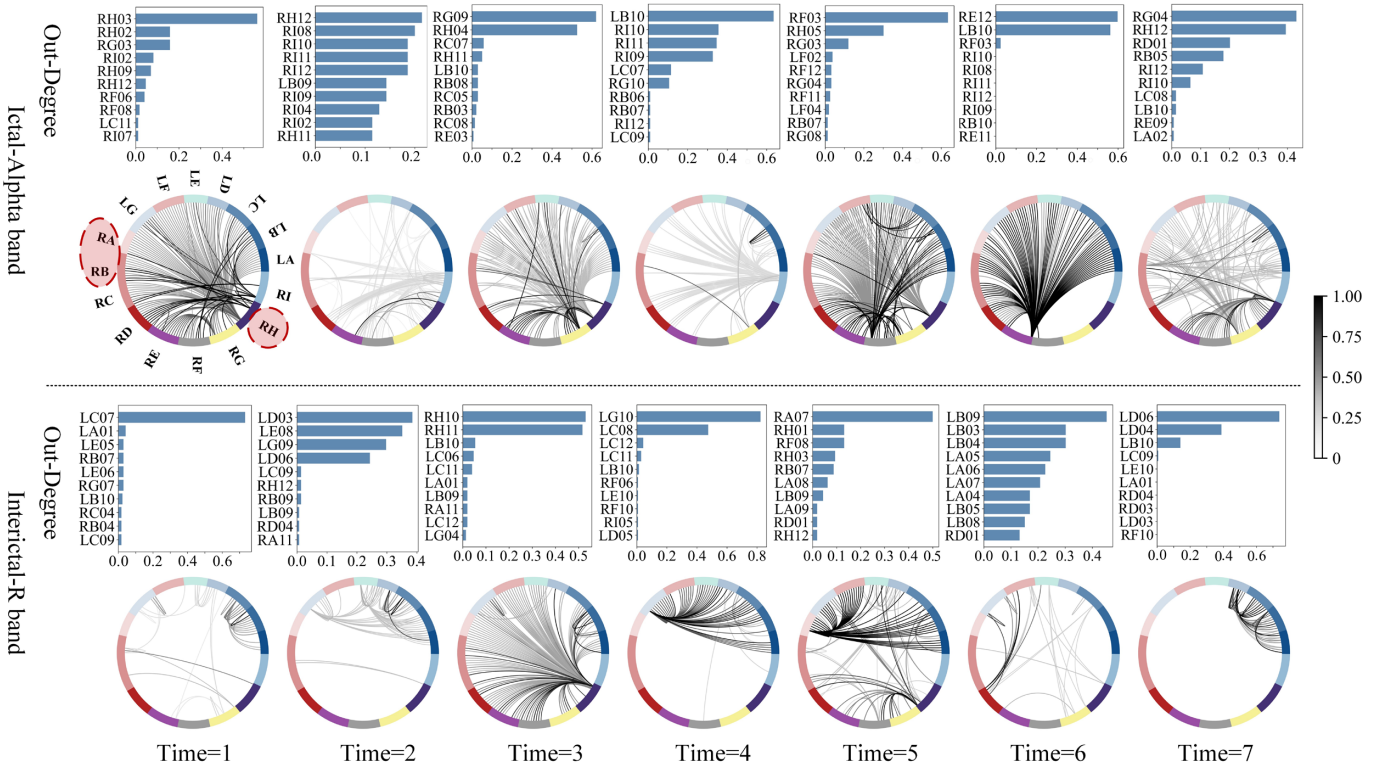


**Fig. 9.** The top 200 important difference edges between ictal and interictal period, learned by the DynSeizureGAT. First, we select the frequency bands with the significant differences, such as, the alpha band in ictal and the R band in interictal to analyze spatial differences of HUP177. Then, the spatial attention weight is extracted after the model's GATv2 and pooling layer, and take the top 200 edges. Moreover, to assist readers with the direction of the information flow, we sort the out-degree of each contact in each network and take the top 10 contacts. 7 second SEEG is used, and the red ellipse represents the epileptogenic regions, with the depth of edge color indicating the size of the edge weight value.

studies indicating that the fast ripple (FR) band is significantly enhanced during the interictal period, and the high-frequency range is notably synchronized, suggesting that FR is a biomarker of the epileptogenic brain [52].

Overall, we observe that DynSeizureGAT effectively learns different frequency bands associated with each patient, and the internal mechanisms of DynSeizureGAT in spectral analysis align with known epileptic seizure patterns.

**2) Interpretation on Spatial-Temporal Properties:** As shown in Fig. 9, we visualize the spatial features obtained through model learning to analyze key edges. First, analyze spatial differences of different periods more specific, the frequency bands with the significant differences in HUP177 from Fig. 8 are selected: the alpha band in the ictal and the R band in the interictal period. Then, the spatial attention weight is extracted after the model's GATv2 and pooling layers, and the top 200 edges are sorted based on weight values to evaluate the differences. Moreover, to assist readers with the direction of the information flow, we sort the out-degree of each contact in each network and take the top 10 contacts. Additionally, to ensure consistency with the model training process, a continuous 7-second SEEG is used for interpretation and analysis.

In Fig. 9, during the ictal period (time1-2), the connection between the temporal lobe epileptogenic region RH (right temporal pole-middle temporal gyrus) and the distal brain area RG (right orbitofrontal cortex-middle frontal gyrus), as well as the contralateral hemisphere area (e.g., LA-LG), is enhanced. In time 3-4, information flows from RG and LB to the epileptogenic zone and other regions. In time5-6, more extensive information flow characteristics are observed. The observation of figure is align with the latest research in epilepsy clinics [48]. During ictal, information flows from the epileptogenic zone to hypoperfused, hyperperfused, and baseline-perfused regions. During ictal evolution, information flows from hypoperfused regions to the epileptogenic zone and hyperperfused and baseline-perfused regions. This reflects the extensive network diffusion observed during epileptic seizures.

During the interictal period, the connection for time3 and time5 shows strong information flow, indicating that high-frequency discharges spread from the RH and RA (right amygdala-middle temporal gyrus) regions to other structures. At other times, information flows in the contralateral brain region but does not spread to the RH and RA region. This observation is consistent with the known pathophysiology [7, 48], demonstrating that the connection pattern during the interictal period remains relatively stable, with information flow primarily occurring unidirectionally from the medial temporal lobe region (e.g., the amygdala) to other structures.

The above analysis reaffirms that DynSeizureGAT effectively captures the dynamic abnormal connectivity patterns unique to epileptic seizure events.

### C. Limitations and future work

Although our proposed method provides more accurate and explainable seizure detection, there are still some limitations. Firstly, even for invasive SEEG, the accuracy is still insufficient for seizure detection tasks. More patients and data are needed, including Engel II to IV patients. Secondly, significant contacts cannot be directly given. Thus, future research will deeply

explore the impact of specific nodes on epileptogenic brain localization by designing a node mask perturbation model, expanding the DRE seizure detection task to the localization of epileptogenic brain regions. Moreover, we will further explore dynamic spatial connectivity biomarkers associated with temporal lobe subtypes of DRE. By investigating generalized patterns of dynamic spatial connectivity, we aim to enhance the clinical diagnostic precision of seizure detection and localization. Fourthly, we will investigate imbalance-aware learning strategies to further improve model generalizability under clinical data distributions.

## VI. CONCLUSION

In this study, we propose a novel multi-band dynamic graph attention network, DynSeizureGAT, to detect and analyze DRE seizures with precision and interpretability. First, a seizure network sequence is constructed by integrating a multi-band directed transfer function matrix and enhanced epileptic index node features. Second, a dynamic graph attention module is integrated to dynamically weigh the contribution of various spatial scales. Third, spatial-spectral-temporal attention mechanisms enhance the model's capacity to better characterize and interpret the ictal and interictal states. Extensive experiments are conducted on the large-scale public clinical SEEG dataset (OpenNeuro). The proposed model demonstrates high seizure detection performance, achieving an average of 94.6% accuracy, 93.4% sensitivity, and 96.4% specificity. Besides the technological innovations, DynSeizureGAT can find abnormal connection patterns, by visualizing the dynamic connection changes of pathological brain networks, which corresponds with seizure propagation mechanisms. It is also expected to assist in locating the epileptogenic brain and provide a scientific method for resection and ablation surgery.

## REFERENCES

- [1] E. Perucca, P. Perucca, H. S. White, and E. C. Wirrell, “Drug resistance in epilepsy,” *The Lancet Neurology*, vol. 22, no. 8, pp. 723–734, 2023/08/01, 2023.
- [2] B. Sultana, M.-A. Panzini, A. Veilleux Carpentier, J. Comtois, B. Rioux, G. Gore, P. R. Bauer, C.-S. Kwon, N. Jetté, C. B. Josephson, and M. R. Keezer, “Incidence and prevalence of drug-resistant epilepsy: a systematic review and meta-analysis,” *Neurology*, vol. 96, no. 17, pp. 805–817, 2021.
- [3] W. H. Organization, “Epilepsy: a public health imperative,” 2019.
- [4] S. Rheims, M. R. Sperling, and P. Ryvlin, “Drug-resistant epilepsy and mortality—Why and when do neuromodulation and epilepsy surgery reduce overall mortality,” *Epilepsia*, vol. 63, no. 12, pp. 3020–3036, 2022/12/01, 2022.
- [5] R. Gadot, G. Korst, B. Shofty, J. R. Gavvala, and S. A. Sheth, “Thalamic stereoelectroencephalography in epilepsy surgery: a scoping literature review,” *Journal of Neurosurgery*, vol. 137, no. 5, pp. 1210–1225, 2022.
- [6] P. S. Reif, A. Strzelczyk, and F. Rosenow, “The history of invasive EEG evaluation in epilepsy patients,” *Seizure - European Journal of Epilepsy*, vol. 41, pp. 191–195, 2016.
- [7] J. M. Bernabeu, A. Li, A. Y. Revell, R. J. Smith, K. M. Gunnarsdottir, I. Z. Ong, K. A. Davis, N. Sinha, S. Sarma, and B. Litt, “Quantitative approaches to guide

- [8] epilepsy surgery from intracranial EEG," *Brain*, vol. 146, no. 6, pp. 2248-2258, Jun 1, 2023.
- [9] Y. Wang, Y. Yang, S. Li, Z. Su, J. Guo, P. Wei, J. Huang, G. Kang, and G. Zhao, "Automatic Localization of Seizure Onset Zone Based on Multi-Epileptogenic Biomarkers Analysis of Single-Contact from Interictal SEEG," *Bioengineering*, vol. 9, no. 12, pp. 769, 2022.
- [10] S. Liu, C. Gurses, Z. Sha, M. M. Quach, A. Sencer, N. Bebek, D. J. Curry, S. Prabhu, S. Tummala, T. R. Henry, and N. F. Ince, "Stereotyped high-frequency oscillations discriminate seizure onset zones and critical functional cortex in focal epilepsy," *Brain*, vol. 141, no. 3, pp. 713-730, Mar 1, 2018.
- [11] J. Li, O. Grinenko, J. C. Mosher, J. Gonzalez-Martinez, R. M. Leahy, and P. Chauvel, "Learning to define an electrical biomarker of the epileptogenic zone," *Human Brain Mapping*, vol. 41, no. 2, pp. 429-441, Feb 1, 2020.
- [12] F. Bartolomei, S. Lagarde, F. Wendling, A. McGonigal, V. Jirsa, M. Guye, and C. Bénar, "Defining epileptogenic networks: contribution of SEEG and signal analysis," *Epilepsia*, vol. 58, no. 7, pp. 1131-1147, 2017.
- [13] M. S. Akter, M. R. Islam, Y. Iimura, H. Sugano, K. Fukumori, D. Wang, T. Tanaka, and A. Cichocki, "Multiband entropy-based feature-extraction method for automatic identification of epileptic focus based on high-frequency components in interictal iEEG," *Scientific Reports*, vol. 10, no. 1, pp. 7044, Apr 27, 2020.
- [14] D. M. Shama, J. Jing, and A. Venkataraman, "DeepSOZ: A Robust Deep Model for Joint Temporal and Spatial Seizure Onset Localization from Multichannel EEG Data," *Medical Image Computing and Computer Assisted Intervention – MICCAI 2023, Lecture Notes in Computer Science*, pp. 184-194, 2023.
- [15] J. Xu, Q. Bian, X. Li, A. Zhang, Y. Ke, M. Qiao, W. Zhang, W. K. J. Sim, and B. Gulyas, "Contrastive Graph Pooling for Explainable Classification of Brain Networks," *IEEE Trans Med Imaging*, vol. PP, Apr 24, 2024.
- [16] Y. Du, Q. Fan, C. Chang, X. Bai, T. Cao, Y. Zhang, X. Wang, and P. Xie, "Characteristics of multi-channel intermuscular directional coupling based on time-varying partial directional coherence analysis," *Scientific Reports*, vol. 13, no. 1, pp. 17088, 2023.
- [17] S. Ma, C. Dong, T. Jia, P. Ma, Z. Xiao, X. Chen, and L. Zhang, "A feature extraction algorithm of brain network of motor imagination based on a directed transfer function," *Computational Intelligence and Neuroscience*, vol. 2022, no. 1, pp. 4496992, 2022.
- [18] A. Ekhlaei, A. M. Nasrabadi, and M. Mohammadi, "Analysis of EEG brain connectivity of children with ADHD using graph theory and directional information transfer," *Biomedical Engineering/Biomedizinische Technik*, vol. 68, no. 2, pp. 133-146, 2023.
- [19] K. Dong, D. Zhang, Q. Wei, G. Wang, X. Chen, L. Zhang, and J. Liu, "An integrated information theory index using multichannel EEG for evaluating various states of consciousness under anesthesia," *Computers in Biology and Medicine*, vol. 153, pp. 106480, 2023.
- [20] D. Klepl, M. Wu, and F. He, "Graph Neural Network-Based EEG Classification: A Survey," *IEEE Transactions on Neural Systems and Rehabilitation Engineering*, vol. 32, pp. 493-503, 2024.
- [21] Y. Liu, Y. Lin, Z. Jia, Y. Ma, and J. Wang, "Representation based on ordinal patterns for seizure detection in EEG signals," *Computers in Biology and Medicine*, vol. 126, pp. 104033, 2020.
- [22] Y. Gao, X. Wang, T. Potter, J. Zhang, and Y. Zhang, "Single-trial EEG emotion recognition using Granger Causality/Transfer Entropy analysis," *Journal of Neuroscience Methods*, vol. 346, pp. 108904, 2020.
- [23] Y. Wang, Y. Dai, Z. Liu, J. Guo, G. Cao, M. Ouyang, D. Liu, Y. Shan, G. Kang, and G. Zhao, "Computer-aided intracranial EEG signal identification method based on a multi-branch deep learning fusion model and clinical validation," *Brain Sciences*, vol. 11, no. 5, pp. 615, May 11, 2021.
- [24] R. Li, X. Yuan, M. Radfar, P. Marendy, W. Ni, T. J. O'Brien, and P. M. Casillas-Espinosa, "Graph signal processing, graph neural network and graph learning on biological data: a systematic review," *IEEE Reviews in Biomedical Engineering*, vol. 16, pp. 109-135, 2021.
- [25] M. Diykh, Y. Li, and P. Wen, "EEG sleep stages classification based on time domain features and structural graph similarity," *IEEE Transactions on Neural Systems and Rehabilitation Engineering*, vol. 24, no. 11, pp. 1159-1168, 2016.
- [26] G. Peng, M. Nourani, H. Dave, and J. Harvey, "Modeling and analysis of seizure network using SEEG for pre-surgery evaluation," in *2022 IEEE 22nd International Conference on Bioinformatics and Bioengineering (BIBE)*, 2022, pp. 327-332.
- [27] G. Wang, D. Wang, C. Du, K. Li, J. Zhang, Z. Liu, Y. Tao, M. Wang, Z. Cao, and X. Yan, "Seizure Prediction Using Directed Transfer Function and Convolution Neural Network on Intracranial EEG," *IEEE Trans Neural Syst Rehabil Eng*, vol. 28, no. 12, pp. 2711-2720, Dec, 2020.
- [28] X. Zhou, C. Liu, R. Yang, L. Zhang, L. Zhai, Z. Jia, and Y. Liu, "Learning robust global-local representation from EEG for neural epilepsy detection," *IEEE Transactions on Artificial Intelligence*, 2024.
- [29] D. Klepl, F. He, M. Wu, D. J. Blackburn, and P. Sarrigiannis, "Adaptive Gated Graph Convolutional Network for Explainable Diagnosis of Alzheimer's Disease Using EEG Data," *IEEE Trans Neural Syst Rehabil Eng*, vol. 31, pp. 3978-3987, 2023.
- [30] K. Zheng, B. Ma, and B. Chen, "DynBrainGNN: Towards Spatio-Temporal Interpretable Graph Neural Network Based on Dynamic Brain Connectome for Psychiatric Diagnosis," *Machine Learning in Medical Imaging, Lecture Notes in Computer Science*, pp. 164-173, 2024.
- [31] J. Guo, T. Feng, P. Wei, J. Huang, Y. Yang, Y. Wang, G. Cao, Y. Huang, G. Kang, and G. Zhao, "Adaptive graph learning with SEEG data for improved seizure localization: Considerations of generalization and simplicity," *Biomedical Signal Processing and Control*, vol. 101, pp. 107148, 2025/03/01/, 2025.
- [32] Y. Dou, J. Xia, M. Fu, Y. Cai, X. Meng, and Y. Zhan, "Identification of epileptic networks with graph convolutional network incorporating oscillatory activities and evoked synaptic responses," *NeuroImage*, vol. 284, pp. 120439, 2023.
- [33] Y. Wang, Y. Shi, Y. Cheng, Z. He, X. Wei, Z. Chen, and Y. Zhou, "A Spatiotemporal Graph Attention Network Based on Synchronization for Epileptic Seizure Prediction," *IEEE J Biomed Health Inform*, vol. 27, no. 2, pp. 900-911, Feb, 2023.
- [34] J. He, J. Cui, G. Zhang, M. Xue, D. Chu, and Y. Zhao, "Spatial-temporal seizure detection with graph attention network and bi-directional LSTM

- architecture," *Biomedical Signal Processing and Control*, vol. 78, 2022.
- [34] Y. Gao, N. Lewis, V. D. Calhoun, and R. L. Miller, "Interpretable LSTM model reveals transiently-realized patterns of dynamic brain connectivity that predict patient deterioration or recovery from very mild cognitive impairment," *Comput Biol Med*, vol. 161, pp. 107005, Jul, 2023.
- [35] S. Brody, U. Alon, and E. Yahav, "How attentive are graph attention networks?", *arXiv preprint arXiv:2105.14491*, 2021.
- [36] J. Shen, J. Chen, Y. Ma, Z. Cao, Y. Zhang, and B. Hu, "Explainable Depression Recognition from EEG Signals via Graph Convolutional Network," in 2023 IEEE International Conference on Bioinformatics and Biomedicine (BIBM), 2023, pp. 1406-1412.
- [37] L. Yang, C. Qiao, H. Zhou, V. D. Calhoun, J. M. Stephen, T. W. Wilson, and Y. Wang, "Explainable Multimodal Deep Dictionary Learning to Capture Developmental Differences From Three fMRI Paradigms," *IEEE Trans Biomed Eng*, vol. 70, no. 8, pp. 2404-2415, Aug, 2023.
- [38] M. Goettling, A. Hammer, H. Malberg, and M. Schmidt, "xEKGArch: a trustworthy deep learning architecture for interpretable ECG analysis considering short-term and long-term features," *Sci Rep*, vol. 14, no. 1, pp. 13122, Jun 7, 2024.
- [39] I. Ahmad, M. Zhu, G. Li, D. Javeed, P. Kumar, and S. Chen, "A Secure and Interpretable AI for Smart Healthcare System: A Case Study on Epilepsy Diagnosis Using EEG Signals," *IEEE J Biomed Health Inform*, vol. 28, no. 6, pp. 3236-3247, Jun, 2024.
- [40] S. Zhang, J. Wang, S. Yu, R. Wang, J. Han, S. Zhao, T. Liu, and J. Lv, "An explainable deep learning framework for characterizing and interpreting human brain states," *Med Image Anal*, vol. 83, pp. 102665, Jan, 2023.
- [41] M. F. Pinto, J. Batista, A. Leal, F. Lopes, A. Oliveira, A. Dourado, S. I. Abuhaiba, F. Sales, P. Martins, and C. A. Teixeira, "The goal of explaining black boxes in EEG seizure prediction is not to explain models' decisions," *Epilepsia Open*, vol. 8, no. 2, pp. 285-297, Jun, 2023.
- [42] A. Li, C. Huynh, Z. Fitzgerald, I. Cajigas, D. Brusko, J. Jagid, A. O. Claudio, A. M. Kanner, J. Hopp, and S. Chen, "Neural fragility as an EEG marker of the seizure onset zone," *Nature neuroscience*, vol. 24, no. 10, pp. 1465-1474, 2021.
- [43] J. M. Bernabei, N. Sinha, T. C. Arnold, E. Conrad, I. Ong, A. R. Patnaik, J. M. Stein, R. T. Shinohara, T. H. Lucas, and D. S. Bassett, "Normative intracranial EEG maps epileptogenic tissues in focal epilepsy," *Brain*, vol. 145, no. 6, pp. 1949-1961, 2022.
- [44] Y. Wang, Y. Yang, G. Cao, J. Guo, P. Wei, T. Feng, Y. Dai, J. Huang, G. Kang, and G. Zhao, "SEEG-Net: An explainable and deep learning-based cross-subject pathological activity detection method for drug-resistant epilepsy," *Computers in Biology and Medicine*, pp. 105703, 2022.
- [45] J. Guo, Y. Wang, Y. Yang, and G. Kang, "IEEG-TCN: a concise and robust temporal convolutional network for intracranial electroencephalogram signal," in IEEE International Conference on Bioinformatics & Biomedicine 2021(BIBM 2021), 2021, pp. 668-673.
- [46] D. Grattarola, L. Livi, C. Alippi, R. Wennberg, and T. A. Valiante, "Seizure localisation with attention-based graph neural networks," *Expert Systems with Applications*, vol. 203, pp. 117330, 2022/10/01/, 2022.
- [47] L. Van der Maaten, and G. Hinton, "Visualizing data using t-SNE," *Journal of machine learning research*, vol. 9, no. 11, 2008.
- [48] B. Frauscher, D. Mansilla, C. Abdallah, A. Astner-Rohracher, S. Beniczky, M. Brazdil, V. Gnatkovsky, J. Jacobs, G. Kalamangalam, and P. Perucca, "Learn how to interpret and use intracranial EEG findings," *Epileptic disorders: international epilepsy journal with videotape*, vol. 26, no. 1, pp. 1-59, 2024.
- [49] F. Wendling, A. Hernandez, J.-J. Bellanger, P. Chauvel, and F. Bartolomei, "Interictal to ictal transition in human temporal lobe epilepsy: insights from a computational model of intracerebral EEG," *Journal of Clinical Neurophysiology*, vol. 22, no. 5, pp. 343-356, 2005.
- [50] X. Fan, N. Gaspard, B. Legros, F. Lucchetti, R. Ercek, and A. Nonclercq, "Dynamics underlying interictal to ictal transition in temporal lobe epilepsy: insights from a neural mass model," *European Journal of Neuroscience*, vol. 47, no. 3, pp. 258-268, 2018.
- [51] B. Frauscher, F. Bartolomei, K. Kobayashi, J. Cimbaliuk, M. A. van 't Klooster, S. Rampp, H. Otsubo, Y. Höller, J. Y. Wu, and E. Asano, "High-frequency oscillations: the state of clinical research," *Epilepsia*, vol. 58, no. 8, pp. 1316-1329, 2017.
- [52] W. Zweiphenning, N. von Ellenrieder, F. Dubeau, L. Martineau, L. Minotti, J. A. Hall, S. Chabardes, R. Dudley, P. Kahane, J. Gotman, and B. Frauscher, "Correcting for physiological ripples improves epileptic focus identification and outcome prediction," *Epilepsia*, vol. 63, no. 2, pp. 483-496, Dec 16, 2021.